Acta Geotechnica
https://doi.org/10.1007/s11440-024-02333-9

RESEARCH PAPER

Correlation of fabric parameters and characteristic features of granular material behaviour in DEM in constitutive modelling

Farid Khayyer[1,2] · Md Mizanur Rahman[2] · Md Rajibul Karim[2]

Received: 20 May 2023 / Accepted: 23 March 2024

Abstract

The anisotropic microstructure of granular materials has a profound effect on their macroscopic behaviour and can be characterised using a fabric tensor. To include of fabric in the critical state theory (CST), anisotropic critical state theory (ACST) was proposed by modifying the state parameter (ψ) of CST to a fabric-dependent dilatancy state parameter (ζ). Noteworthy that ψ showed a very strong correlation with characteristic features (e.g. instability, phase transformation and characteristic state) of macroscopic behaviour and, as a result, it has been adopted in many constitutive models. While ζ aided the inclusion of fabric in ACST models, the correlation between ζ and characteristic features has not been evaluated in detail yet, although a large number of works are found on micromechanics and fabric only. In this study, a large number of discrete element method simulations for drained and undrained triaxial were conducted to evaluate the correlation between ζ and characteristic features. To this purpose, the correlation between stress ratio and both classic and dilatancy state parameter (ψ and ζ) were studied in important characteristic features (e.g. instability, phase transformation and characteristic state). It was found that this correlation was improved using ζ which might be due to the inclusion of fabric in our model. This observation is new and significant for inclusion of fabric evolution in constitutive modelling.

Keywords Critical state · DEM · Dilatancy · Fabric

List of symbols

A	Fabric anisotropic variable (FAV)
A'	A measure of the relative orientation of F_{ij} and n_{ij}
C_n	Local damping coefficient
D_P	Stress dilatancy
δ_{ij}	The Kronecker delta
Λ, ξ	Fitting parameters in Eq. (3)
e	Void ratio
e_0	Initial void ratio (void ratio before shearing)
e_c	Critical void ratio
e_{CS}	Void ratios on the CSL at p'
e_{lim}	Void ratio on CSL at p = 0 kPa
ε_1	Axial strain
ε_q^p	Deviator strain (plastic)
ε_v^p	Volumetric strain (plastic)
η	Stress ratio
η_c	Stress ratio at critical state
F	Fabric intensity
F_0	Initial fabric
F_{11}, F_{22}, F_{33}	Fabric tensors in three orthogonal directions
F_{12}, F_{13}, F_{23}	Fabric tensors in the shear directions
F_{ij}	Fabric tensor
F_{vm}	von Mises fabric invariant
$g(\theta)$	Interpolation function based on the Lode angle θ
K_F	Stress-fabric joint invariant
K_n	Normal contact stiffness, $K_n = K_0 \times r$, where K_0=1 × 10^5
K_s	Shear contact stiffness
M	Intrinsic material property corresponding to stress ratio at critical state
M_e	Critical state stress ratio in triaxial extension

✉ Md Mizanur Rahman
Mizanur.Rahman@unisa.edu.au

Farid Khayyer
Farid.khayyer@mymail.unisa.edu.au

Md Rajibul Karim
Rajibul.Karim@unisa.edu.au

[1] Tonkin + Taylor Pty Ltd, Southbank, Australia

[2] UniSA STEM, University of South Australia, Adelaide, SA 5000, Australia

Published online: 11 May 2024

M_c	Critical state stress ratio in triaxial compression
μ	Interparticle friction coefficient
N	Number of contacts in the specimen
N_P	Number of particles
n_{ij}	Deviatoric loading direction
n_{ij}^F	Deviatoric fabric direction
n_i^c	Unit vector along the normal direction of the contact plane
ν	Poisson's ratio
p'	Mean effective stress
p'_0	Initial confining pressure
p_a	Atmospheric pressure
φ_{ij}	Fabric tensor
ψ	State parameter
ψ_0	Initial state parameter
ψ_{0-DEM}	Initial state parameter from micromechanics entities of this DEM Study
ψ_{0-CM}	Initial state parameter calculated by constitutive formulation
q	Deviator stress
r	Particle radius
s_{ij}	Deviatoric stress tensor
σ'_1, σ'_3	Major principal effective stresses in triaxial condition
σ_{ij}	Stress tensor
θ	The Lode angle
Z_m	Mechanical coordination number
ζ	Dilatancy state parameter
ζ_0	Initial dilatancy state parameter
ζ_{0-DEM}	Initial dilatancy state parameter from micromechanics entities of this DEM Study
ζ_{0-CM}	Initial dilatancy state parameter calculated by constitutive formulation

1 Introduction

When a soil element is continuously sheared, it eventually flows as a frictional fluid and reaches a well-defined critical state, CS [64, 68]. Schofield, Wroth [68], in their definition of CS, did not make any reference to fabric-related entities other than the scalar-valued void ratio (e). Therefore, the CS was fabric independent, i.e. based on fabric isotropy. These CSs from many tests/conditions form a unique critical state line (CSL), which is taken as the reference line to understand/predict a soil element's behaviour within the critical state soil mechanics (CSSM) framework. Such a fabric-independent CS and CSL proved to be sufficient for many loading conditions for many soils. A mathematical definition of such a CSL, in terms of mean effective stress (p'), deviatoric stress (q) and void ratio (e), can be presented by

$$\eta = \eta_c = (q/p')_c = M \tag{1}$$

$$e = e_c = \widehat{e}_c(p') \tag{2}$$

where, M is the ratio of q and p' at CS, which is a constant and intrinsic material property. $e_c = \widehat{e}_c(p')$ is the critical state void ratio expressed as the function of p' in $e - \log(p')$ space. For conventional triaxial tests, the p' and q can be simplified to $p' = (\sigma'_1 + 2\sigma'_3)/3$ and $q = (\sigma'_1 - \sigma'_3)$, respectively; where, σ'_1 and σ'_3 are the axial stress and effective radial stresses, respectively. Equations (1) and (2) define a unique CSL in e-q-p' space. Often, as in this paper, the name CSL is used to denote the line in the e-p' space, expressed by the following power function as proposed by Li and Wang [34]:

$$e_c = \widehat{e}_c(p') = e_{lim} - \Lambda\left(\frac{p'}{p_a}\right)^{\xi} \tag{3}$$

where, e_{lim} is the void ratio on CSL at p' = 1 kPa, Λ and ξ are fitting parameters and p_a is atmospheric pressure of 100 kPa. A soil element's behaviour in shearing is controlled by its current state in relation to its reference state, i.e. CSL. For example, if a soil element state is above the CSL in e-p'space, the soil state moves leftward to meet CSL during undrained shearing. As a result, soil element exhibits contractive behaviour. On the other hand, if the state of the soil element is below the CSL, then during undrained shearing, the state moves rightward to meet CSL. As a result, soil element displays dilative behaviour. Many researchers realised this attribute [e.g. 4,5–7], and they tried to evaluate it by different measures of states such as state parameter [4], state index [19], stress ratio [26], pressure index [79], and modified state parameter [5]. Among these measures, the most commonly used parameter is the state parameter ψ suggested by Been, Jefferies [4]. ψ is the difference of void ratio at the current (e) state and critical state (e_c) at the same p'. This can be presented by the following equation:

$$\psi = e - e_c \tag{4}$$

It was found that ψ correlate with characteristic behaviours of granular materials, e.g. peak failure stress ratio [81], stress ratio at phase transformation (η_{PT}) [38, 90], instability stress ratio (η_{IS}) at peak q [28, 58, 60], cyclic

instability type liquefaction [2, 3, 56, 63]. Therefore, subsequently, ψ is used in constitutive modelling [9, 10, 14, 22, 31, 38, 81] by improving/modifying the correlation of characteristic features as a function of ψ.

However, many studies revealed that the granular soil response during almost all stages of loading history is fabric anisotropic [42, 50, 65, 88]. Therefore, CS without fabric, except for a scalar value of e, may be sufficient in many conditions but cannot be complete. Indeed, when introducing their ψ, Been, Jefferies [4] suggested that the CS in soil may be fabric-dependent or anisotropic. Both experimental and numerical studies attempted to define fabric anisotropy by linking them to the arrangement of soil particles, voids and interparticle contacts and the effect of applied loads on these microstructures [1, 6, 41, 48, 67, 70, 87]. Li, Dafalias [32] proposed a fabric anisotropic variable (A) to capture fabric anisotropy and its fabric evolution as below-

$$A = F_{ij} n_{ij} \tag{5}$$

where, F_{ij} is the deviatoric fabric tensor and n_{ij} is the unit-norm deviatoric tensor-valued direction, both of which are defined later in this study (refer to Sect. 2.2). Li and Dafalias [32] also proposed the anisotropic critical state theory (ACST) by extending the definition of CSL with the inclusion of A in Eq. (6). The third term is the extension of original definition of CSL in Eq. (1) and Eq. (2).

$$\eta = \eta_c = M, \quad e = e_c = \widehat{e}_c(p'), \quad A = A_c = 1 \tag{6}$$

This allows an extension of ψ for fabric with the inclusion of A to the dilatancy state parameter, DSP (ζ). Li, Dafalias [32] used a combined norm of the distance for the current value of both e and A to their corresponding critical state as shown below-

$$\zeta = \psi - \psi_A = \psi - \widehat{e}_A(e, p')(A - 1) \tag{7}$$

where $\widehat{e}_A(e, p')$ is a function on e and p'. However, Li, Dafalias [32] used a constant value for simplicity and left open the possibility for other expressions, in particular, to achieve better simulations while maintaining the basic premises of $\zeta = \psi$ when $A = A_{CS} = 1$ at CS are satisfied. Along this line, Rahman, Dafalias [57] modified the DSP by defining $\widehat{e}_A(e, p')$ as below-

$$\widehat{e}_A(e, p') = e_A \frac{\langle e_{\lim} - e \rangle}{(e_{\lim} - e_c)} \tag{8}$$

where, e_A is a fitting parameter. The Macauley brackets define the operation ‹a› = a for a > 0 and ‹a› = 0 for a ≤ 0. Thus, for ($e_{\lim} - e < 0$), Eq. (7) yields $\zeta = \psi$.

However, further research is needed to verify the above-proposed equation using micromechanical approaches. The main motivation of the current study is to provide further evidence and to evaluate the above model using three-dimensional Discrete Element Method (DEM) simulations.

DEM can be a useful micromechanical tool to understand granular soil anisotropic response and its evolution with loading [35, 39, 44, 47, 48, 75, 80, 83, 93]. It allows the examination of particle-scale interaction, contact, or fabric to establish a link with the macro-response. Many previous studies effectively capture fabric anisotropy evolution but may not directly translate or connect to continuum mechanics, especially within the context of ACST, which is the focus of the current study. In this study, the ψ (classic state parameter without fabric Been, Jefferies [4]), DSP ζ Li, Dafalias [32] and modified DSP ζ [57] were utilised to evaluate their link with characteristic features (e.g. instability, phase transformation and characteristic state) and to explore the effect of microstructural fabric anisotropies on macroscopic shear behaviour. It also enhances understanding of fabric evolution in constitutive modelling.

2 Dem modelling

2.1 Triaxial test simulation

The DEM software, PFC^{3D} [21], was used in this study to perform the numerical simulation. The specimen was represented in a cubic space confined with three pairs of stress or strain-controlled friction-less walls, as shown in Fig. 1a. Wall stiffness should be much larger than particles to avoid unnecessary wall deformation and to ensure constant volume during undrained tests. Therefore, the wall stiffness was 1×10^7 kN/m [21, 30]. The soil particles are modelled as spheres with the particle size distribution (PSD) of Toyoura sand [19] and with a linear force–displacement contact law (see Fig. 1b, c). It should be noted that in definition of the contact model, the force–displacement law is not applied to inactive contacts (refer Fig. 1a for particles with less than two contacts). Non-spherical particles may be a more realistic representation of soil assembly [46, 62], but have not been adopted in this study to avoid intensive computation and excessive complexity. The contact stiffness varied on orders in literature [16, 17, 29, 36, 40, 69, 72, 74]. However, Li [30] showed that the contact stiffness would not have a significant impact on soil behaviour at large strains. In this study, the most commonly used normal and tangential stiffnesses have been adopted as $\frac{k_n}{r} = \frac{k_s}{r} = 10^5$ kN/m^2 [16, 25, 84]. The simulation parameters are summarized in Table 1.

Triaxial specimens, prior to the consolidation, were prepared as the following procedure:

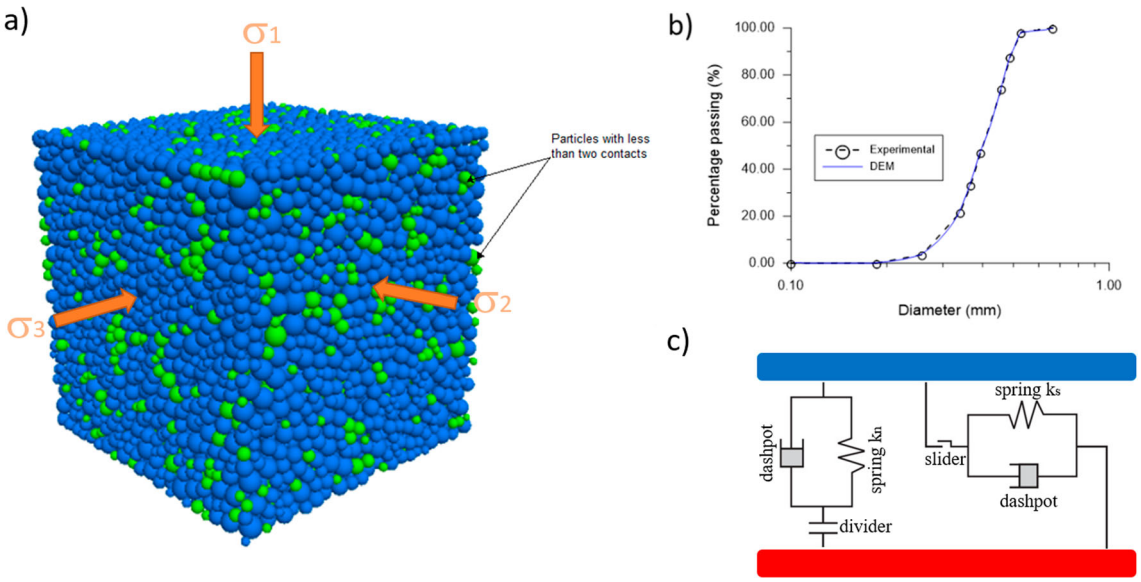

Fig. 1 **a** Specimen with particles in the simulation, **b** particle size distribution, **c** contact model

Table 1 The input parameters of DEM modelling

Particle density (kg/m^3)	2650	Number of particles	13,570 *
Interparticle friction coefficient, μ	0.5	Wall-particle friction	0
Wall stiffness (kN/m)	1×10^7	Normal contact stiffness K_n (kN/m)	$k_n = k_0 \times r$, where $k_0 = 1 \times 10^5$
Local damping coefficient, C_n	0.7	Shear contact stiffness K_s (kN/m)	$K_s = K_n$
Particle size distribution	Toyoura sand		

*The effect of the number of particles are further discussed in the Appendix

- Specimen generation: The random distribution method has been adopted to generate specimens with 13,570 spheres (the effect of the number of particles is discussed in the appendix). Initially, particles overlapped greatly, and strong repulsive forces arose. Therefore, some cycles were needed by the system to reach equilibrium and generate a specimen without overlap. Interparticle friction coefficient (μ) was temporarily set to zero during this stage.
- Initial state: Since all specimens were generated by the same mechanism, therefore the contact forces throughout the assembly are expected to be similar, resulting in an isotropic uniform network of contact forces similar to the radii expansion method [16, 23, 53]. An isotropic stress of 10 kPa by servo control of the walls was applied to the specimen. During this stage, different μ were used to generate specimens with different densities [82, 84]. Generally, a low value of μ generates a dense specimen, while a high μ value generates a loose specimen. This was an effective technique of sample generation since it allows the generation of a homogeneous network of contact forces and particle distribution within the created samples [61]; it is computationally efficient and avoids the onset of high lock-in contact forces.
- Isotropic consolidation: Upon finishing this stage, μ was changed to 0.5, and the specimen was cycled again to an equilibrium state. Now, the specimen was assumed at its initial state and is ready for isotropic consolidation. As summarised in Table 2, a total of 108 specimens have been prepared in different confining pressures under undrained and drained conditions (54 specimens each).
- Monotonic shearing: For the drained triaxial test, the strain-controlled top and bottom walls were compressed (axial strain), while the stresses on the side walls were kept constant using a servo mechanism simulating constant cell pressure. On the other hand, the undrained triaxial test was simulated by a constant volume test, in which the total volume of the specimen remains constant by servo control of the walls and the stresses of the wall are assumed to be effective stresses [21, 30]. Hence, the excess pore water pressure during the shearing equals the difference between the current effective stress and initial confining pressure on the vertical walls.

Table 2 Summary of the test simulations

No	Test ID	e_0	No.	Test ID	e_0
1	CIU-30–0.736	0.736	55	CID-30–0.736	0.736
2	CIU-30–0.726	0.726	56	CID-30–0.726	0.726
3	CIU-30–0.715	0.715	57	CID-30–0.715	0.715
4	CIU-50–0.731	0.731	58	CID-50–0.729	0.729
5	CIU-50–0.721	0.721	59	CID-50–0.721	0.721
6	CIU-50–0.710	0.710	60	CID-50–0.709	0.709
7	CIU-70–0.725	0.725	61	CID-70–0.725	0.725
8	CIU-70–0.716	0.716	62	CID-70–0.715	0.715
9	CIU-70–0.705	0.705	63	CID-70–0.705	0.705
10	CIU-90–0.720	0.720	64	CID-90–0.719	0.719
11	CIU-90–0.711	0.711	65	CID-90–0.710	0.710
12	CIU-90–0.701	0.701	66	CID-90–0.700	0.700
13	CIU-100–0.718	0.718	67	CID-100–0.718	0.718
14	CIU-100–0.709	0.709	68	CID-100–0.708	0.708
15	CIU-100–0.690	0.690	69	CID-100–0.689	0.689
16	CIU-100–0.660	0.660	70	CID-100–0.659	0.659
17	CIU-100–0.631	0.631	71	CID-100–0.630	0.630
18	CIU-100–0.611	0.611	72	CID-100–0.610	0.610
19	CIU-100–0.574	0.574	73	CID-100–0.574	0.574
20	CIU-300–0.675	0.675	74	CID-300–0.674	0.674
21	CIU-300–0.668	0.668	75	CID-300–0.667	0.667
22	CIU-300–0.652	0.652	76	CID-300–0.651	0.651
23	CIU-300–0.626	0.626	77	CID-300–0.625	0.625
24	CIU-300–0.601	0.601	78	CID-300–0.599	0.599
25	CIU-300–0.583	0.583	79	CID-300–0.582	0.582
26	CIU-300–0.549	0.549	80	CID-300–0.548	0.548
27	CIU-500–0.640	0.640	81	CID-500–0.639	0.639
28	CIU-500–0.633	0.633	82	CID-500–0.633	0.633
29	CIU-500–0.619	0.619	83	CID-500–0.619	0.619
30	CIU-500–0.597	0.597	84	CID-500–0.596	0.596
31	CIU-500–0.574	0.574	85	CID-500–0.573	0.573
32	CIU-500–0.557	0.557	86	CID-500–0.556	0.556
33	CIU-500–0.526	0.526	87	CID-500–0.526	0.526
34	CIU-700–0.609	0.609	88	CID-700–0.608	0.608
35	CIU-700–0.603	0.603	89	CID-700–0.602	0.602
36	CIU-700–0.590	0.590	90	CID-700–0.590	0.590
37	CIU-700–0.571	0.571	91	CID-700–0.570	0.570
38	CIU-700–0.549	0.549	92	CID-700–0.547	0.547
39	CIU-700–0.534	0.534	93	CID-700–0.533	0.533
40	CIU-700–0.505	0.505	94	CID-700–0.505	0.505
41	CIU-1000–0.567	0.567	95	CID-1000–0.567	0.567
42	CIU-1000–0.562	0.562	96	CID-1000–0.561	0.561
43	CIU-1000–0.551	0.551	97	CID-1000–0.550	0.550
44	CIU-1000–0.534	0.534	98	CID-1000–0.533	0.533
45	CIU-1000–0.515	0.515	99	CID-1000–0.514	0.514
46	CIU-1000–0.502	0.502	100	CID-1000–0.501	0.501
47	CIU-1000–0.476	0.476	101	CID-1000–0.475	0.475
48	CIU-2000–0.454	0.454	102	CID-2000–0.454	0.454
49	CIU-2000–0.451	0.451	103	CID-2000–0.451	0.451
50	CIU-2000–0.443	0.443	104	CID-2000–0.442	0.442
51	CIU-2000–0.432	0.432	105	CID-2000–0.432	0.432
52	CIU-2000–0.419	0.419	106	CID-2000–0.418	0.418
53	CIU-2000–0.410	0.410	107	CID-2000–0.409	0.409
54	CIU-2000–0.391	0.391	108	CID-2000–0.390	0.390

2.2 Stress tensor and fabric tensor

In order to quantify the macroscale response of a DEM assembly, the stress tensor must be defined in terms of discrete quantities such as particle displacements, contact normal, and contact forces by means of an averaging procedure [37, 51]. In a granular assembly, boundary loads are distributed among the intergranular contacts. The balance between boundary loads and internal forces leads to the expression for stress tensor as proposed by Christoffersen et al. [8]:

$$\sigma_{ij} = \frac{1}{V}\sum_{c\in N_c} f_i^c l_j^c \tag{9}$$

where, σ_{ij} is the stress tensor, V is the volume of the assembly, N_c is all contact points in V, f_i^c is the corresponding force vector between particles, l_i^c is the branch vector joining the centres of two contacted particles. By calculating the stress tensor components, it would be possible to calculate effective confining pressure (p') and deviatoric stress (q) based on Eqs. (10) and (11).

$$p' = \frac{\sigma_{ii}}{3} \tag{10}$$

$$q = \sqrt{\frac{3.s_{ij}s_{ij}}{2}} \tag{11}$$

where, $s_{ij} = \sigma_{ij} - \delta_{ij}p'$ and δ_{ij} is the Kronecker delta.

The spatial distributions (i.e. anisotropies) of the contact normal and contact forces play a significant role in the shear behaviour of granular soil, which can be characterised using fabric tensor in DEM. Among the various definitions of fabric tensor [e.g. 18, 24, 33, 48], the contact normal-based proposition by Satake [67] and Oda [49] was adopted here:

$$\varphi_{ij} = \frac{1}{N}\sum_{c\in N_c} n_i^c n_j^c \tag{12}$$

where, φ_{ij} is the fabric tensor, n_i^c is the unit vector along the normal direction of the contact plane; and N is number of contacts in the specimen.

The deviatoric fabric tensor can also be defined as below:

$$F_{ij} = \varphi_{ij} - \frac{1}{3}\delta_{ij} \tag{13}$$

In order to characterise the fabric anisotropy, a scalar value obtained from deviatoric fabric tensor is usually used to quantify the degree of fabric anisotropy. This scalar value can then be used together with the scalar valued stress ratio ($\eta = q/p'$) and void ratio (e) to define the conditions for a critical state outlined in Eq. (6).

To examine whether the unique critical state features can be identified for fabric anisotropy at CS, a number of variables such as FAV A as expressed by Eq. (5), von Mises invariant (F_{vm}) of fabric tensor proposed by Huang et al. [18] and stress-fabric joint invariant (K_{F}) defined by Zhao and Guo [91] are adopted in this study, all of which are further discussed in the following sections.

3 Results and discussions

3.1 Simulation program

Table 2 summarises the test program in this study. Each test is identified by the loading condition, initial confining pressure (p'_0) and initial void ratio (e_0) of the specimen. For example, CIU-70-0.725 indicates isotropic undrained compression (CIU) test on a specimen that was under a p'_0 of 70 kPa and had an e_0 of 0.725 at the end of consolidation. For the same token, CID means isotropic drained compression test.

3.2 Macromechanical behaviour

The undrained behaviours of specimens with the same p'_0 of 100 kPa but at different e_0 are shown in Fig. 2. All specimens, including in Fig. 2, reached/approached CS at a large strain.

As can be seen in Fig. 2, the typical undrained mechanical behaviours comparable to the experimental observations [76] can be identified in the simulation. CIU-100-0.574, CIU-100-0.631 and CIU-100-0.660 show dilative behaviours, CIU-100-0.709 shows phase-transformation behaviour, and CIU-100-0.718 shows static liquefaction. Accordingly, the specimens with e_0 of 0.574, 0.631 and 0.660 can be considered as very dense to dense specimens, and the specimens with e_0 of 0.709 and 0.718 can be considered as medium dense and very loose specimens, respectively. As expected by the theory of critical state soil mechanics, a unique CSL can be drawn for these states, as shown in Fig. 2b.

The drained behaviours of the specimens with the same p'_0 of 100 kPa but at different e_0 are presented in Fig. 3. The dense specimen exhibits a softening behaviour after reaching an initial peak, whereas the loose specimen shows a continuous hardening behaviour. As expected, all specimens finally reach a unique CS with constant values of e, p' and q by either dilation or contraction.

Figure 4a shows the critical state lines deduced from 108 undrained and drained tests in this study. The best-fit relation can be presented by the power function expressed in Eq. (3) in which $e_{\mathrm{lim}} = 0.723$, $\Lambda = 0.018$ and $\xi = 0.9$. As seen in Fig. 4b, the CS data points can be described by a single line with a slope of 0.78 in q–p' space which is actually the stress ratio, M, as expressed in Eq. (1). These CS parameters will be used in following sections for calculation of classic and dilatancy state parameters.

The above results indicate that the DEM simulations are able to capture all features of the macroscopic density- and pressure-dependent behaviours of granular soils. To explain the macroscopic behaviour at the grain-scale, the microstructure and its evolution during shearing, including contact numbers, contact forces, contacts distribution and microscopic geometry, are discussed using contact- and fabric-based variables in the following sections.

3.3 Micromechanical behaviour

3.3.1 Evolution of contact number

To explain the behaviour of granular soil in micro-scale, the contact density of the model is studied using the mechanical coordination number (Z_{m}). It should be noted that Z_{m} excludes the particles with zero or one contact, as they do not contribute to a stable state of stress during shearing. Particles with less than two contacts are shown in Fig. 1.

Figure 5 shows the evolution of Z_{m} in the undrained and drained tests. As expected, the initial Z_{m} of a specimen increases with increasing initial density. During the undrained tests, the Z_{m} of dense specimens (e_0 = 0.574 and 0.631) decrease rapidly first and thereafter increase gradually with further shearing. Regarding the medium-dense specimen (e_0 = 0.660), the Z_{m} gradually decreases to a minimum value at quasi-steady state and then increases with further shearing due to an increase of p'. For a very loose specimen (e_0 = 0.718), the Z_{m} decreases continuously to a limited value of around 8.0 and then suddenly drops to zero. This can be considered as a sign of soil collapse and the occurrence of static liquefaction. The Z_{m} value of specimens in the drained tests increases slightly first and then decreases continuously until reaching a critical state with identical Z_{m}, which is consistent with numerical observations by Duran [11] and Rothenburg [66].

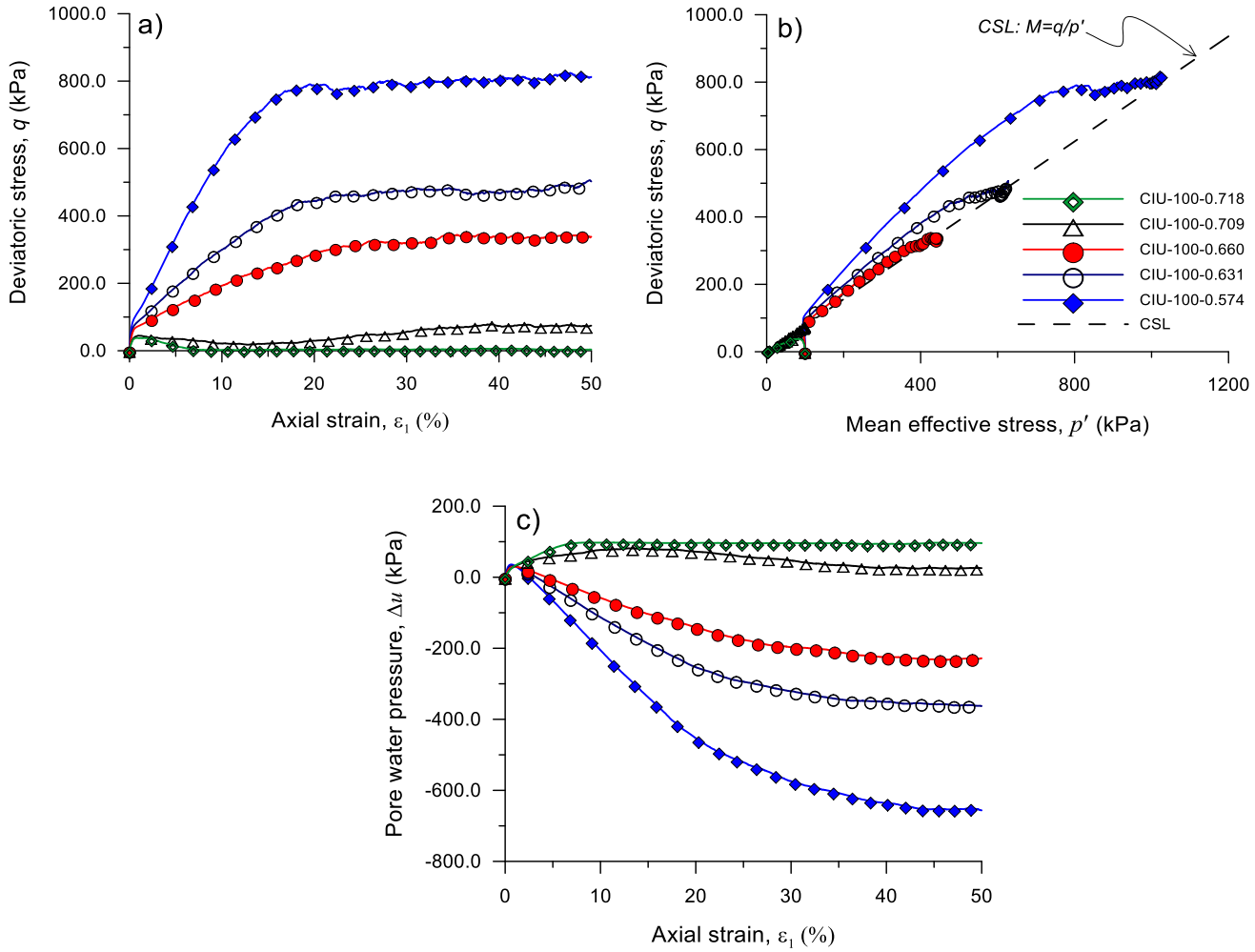

Fig. 2 Undrained behaviours of specimens with different densities: evolutions of **a** deviatoric stress vs ε_1; **b** effective stress path; **c** excess pore water pressure vs ε_1

Therefore, to some extent, coordination number may be an intrinsic variable characterising soil density and instability potential. However, in an undrained test, the Z_m after the instability of a very loose specimen does not make much sense (decreasing while the specimen is contracting). This would suggest that the Z_m cannot solely capture the behaviour of granular soil at the particle scale and shall be combined with fabric anisotropy (i.e. contact normal, contact forces, contact distribution and microscopic geometry) to properly describe the soil density at the particle scale.

3.3.2 Evolution of anisotropies

The structural anisotropy can be characterised by the second-order fabric anisotropy tensor (F_{ij}) as expressed in Eq. (13). A scalar quantity of fabric can be presented by the von Mises fabric (F_{vm}), which is derived from the invariant of F_{ij} as expressed below:

$$F_{vm} = \sqrt{\frac{3}{2} F_{ij} F_{ji}} \tag{14}$$

which can be rewritten as:

$$F_{vm} = \sqrt{\frac{1}{2}\left[(F_{11}-F_{22})^2 + (F_{11}-F_{33})^2 + (F_{22}-F_{33})^2 + 6\left(F_{12}^2 + F_{13}^2 + F_{23}^2\right)\right]} \tag{15}$$

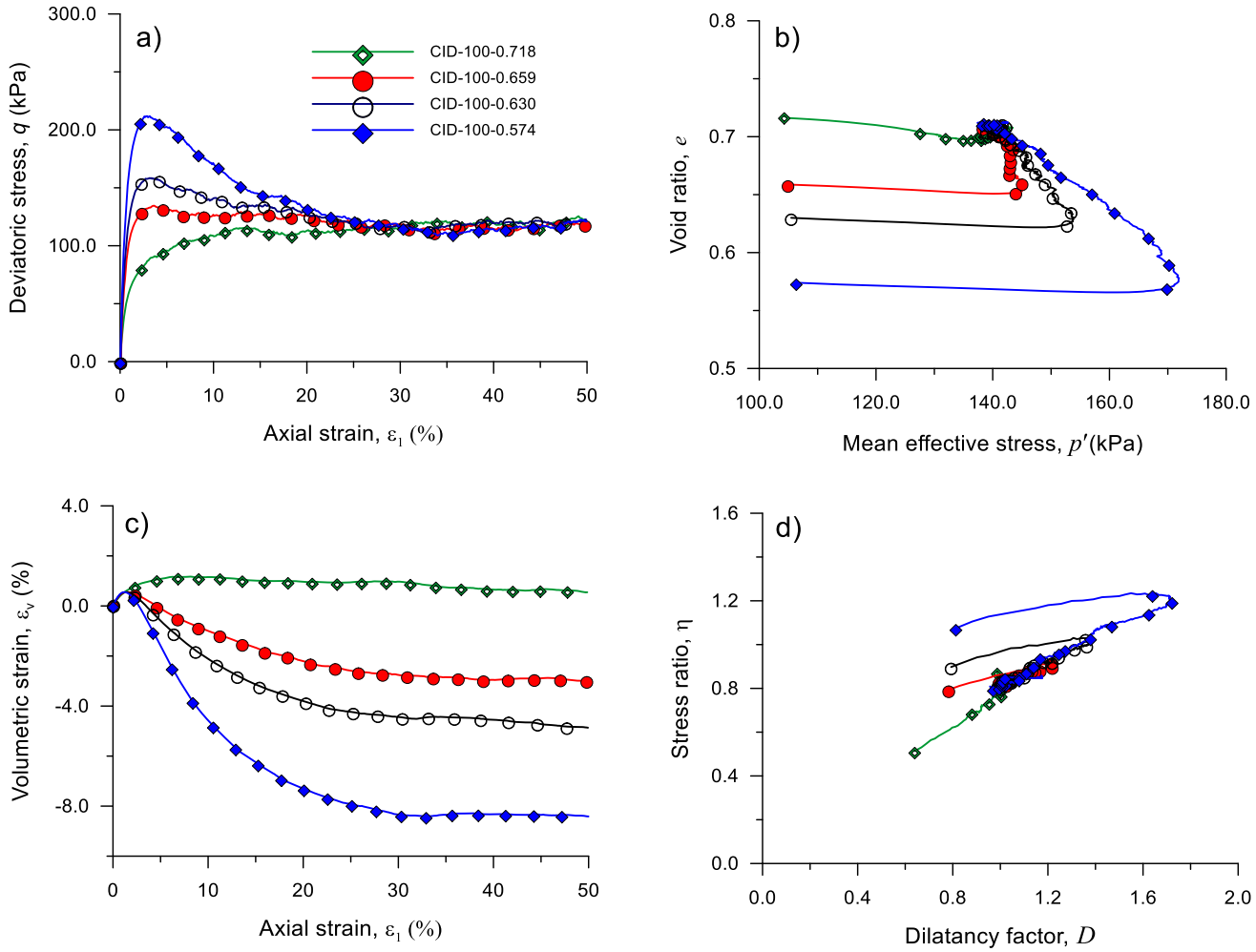

Fig. 3 Drained behaviours of specimens with different densities: evolutions of **a** deviatoric stress vs ε_1; **b** void ratio vs p'; **c** volumetric strain vs ε_1; and **d** stress ratio vs dilatancy factor, D

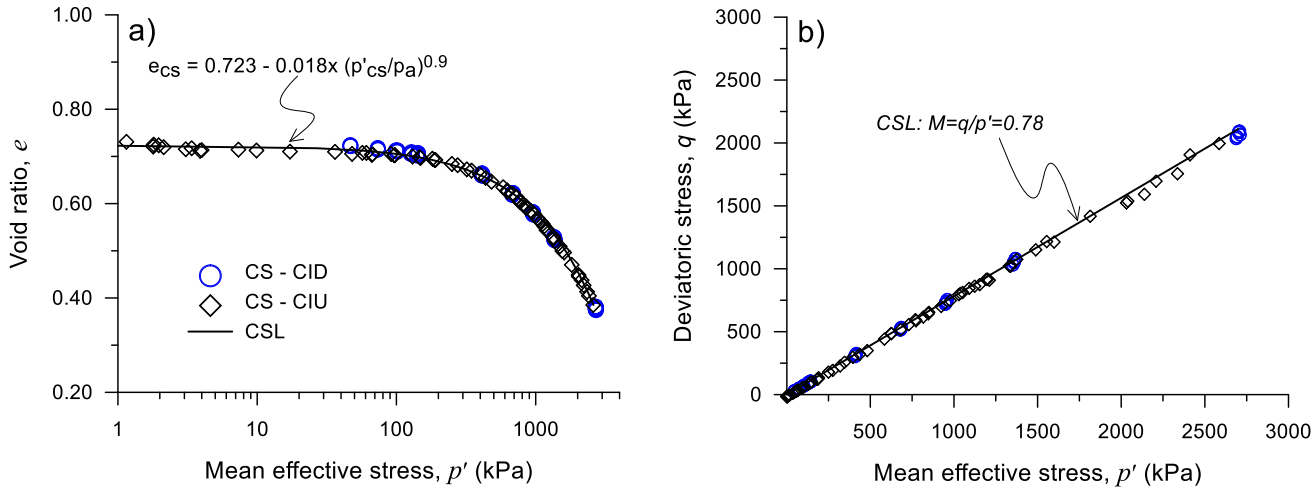

Fig. 4 Critical state lines in **a** $e - p'$ plane and **b** $q - p'$ plane

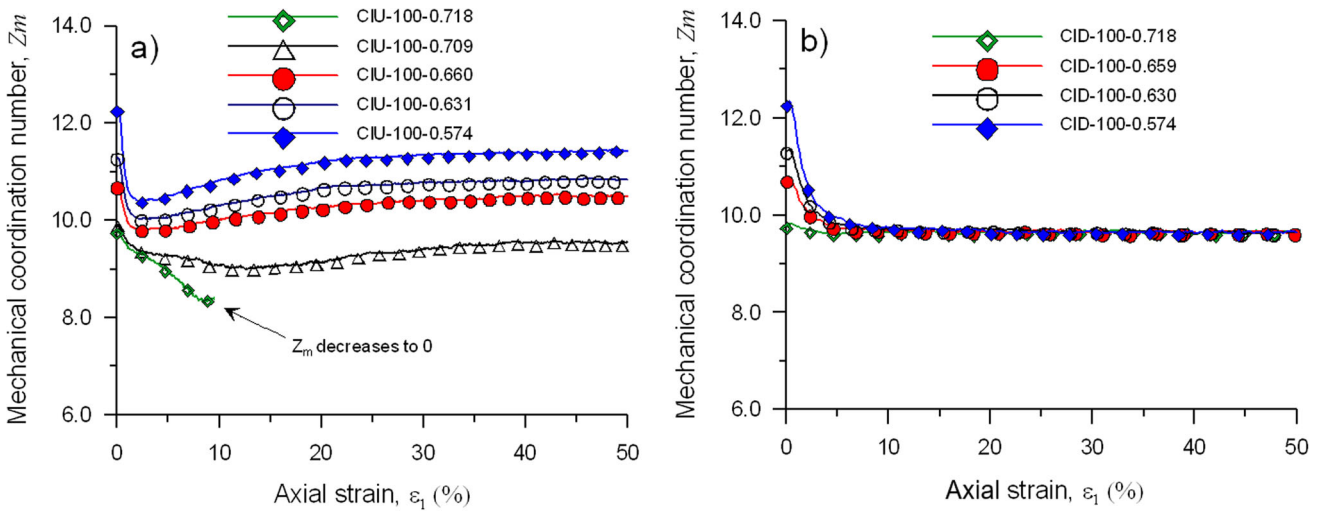

Fig. 5 Evolutions of mechanical coordination numbers Zm vs ε_1 **a** undrained tests; **b** drained tests

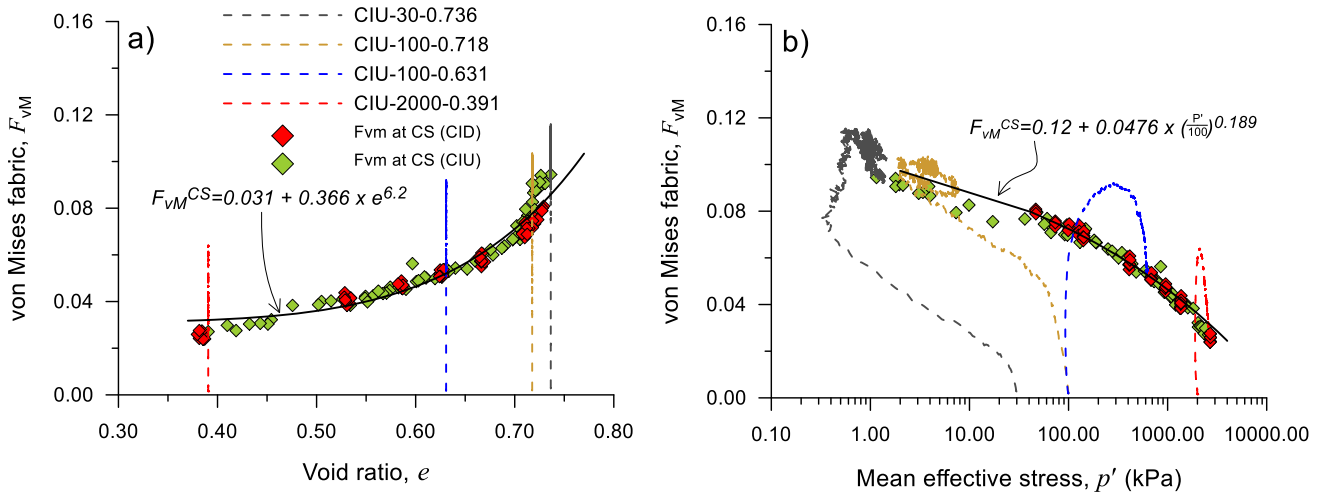

Fig. 6 F_{vM} values at CS and the evolution of F_{vM} during undrained shearing: **a** F_{vM}–p' space; **b** F_{vM}–e space

here, F_{11}, F_{22}, and F_{33} are fabric tensors in three orthogonal directions; and F_{12}, F_{13}, and F_{23} are fabric tensors in the shear directions.

It is interesting to examine whether the unique critical state features can be identified for fabric anisotropy at CS. Figure 6a, b show the relationships between F_{vm} and p' and F_{vm} and e at CS. A non-linear relationship for F_{vm} at CS is observed, which implies the uniqueness of CSL. The evolution of F_{vm} during the undrained shearing process for four samples with different p' is also presented in Fig. 6a, b to demonstrate the stress dependency of the evolution path.

However, as shown by several past studies, fabric anisotropy is intimately related to the loading path and contact forces [e.g. , 1373. Due to this dependency, an anisotropy variable defined based on both loading direction and fabric tensor may offer a more accurate characterisation of soil anisotropies.

Therefore, the following scalar values are also examined in this study:

1. Joint invariant of stress tensor and fabric tensor (K_F) proposed by Zhao and Guo [91]:

$$K_F = s_{ij}F_{ij} \tag{16}$$

where F_{ij} is the deviatoric fabric tensor described by Eq. (13) and s_{ij} is previously defined in Eq. (11).

2. The scalar measure of relative fabric orientation, FAV A of Eq. (5) ($A = F_{ij}n_{ij}$).

where n_{ij} is the deviatoric loading direction, and for monotonic loading conditions in this study, can be defined by a unit-norm deviatoric tensor, n_{ij} along the normal to the yield surface in deviatoric stress space:

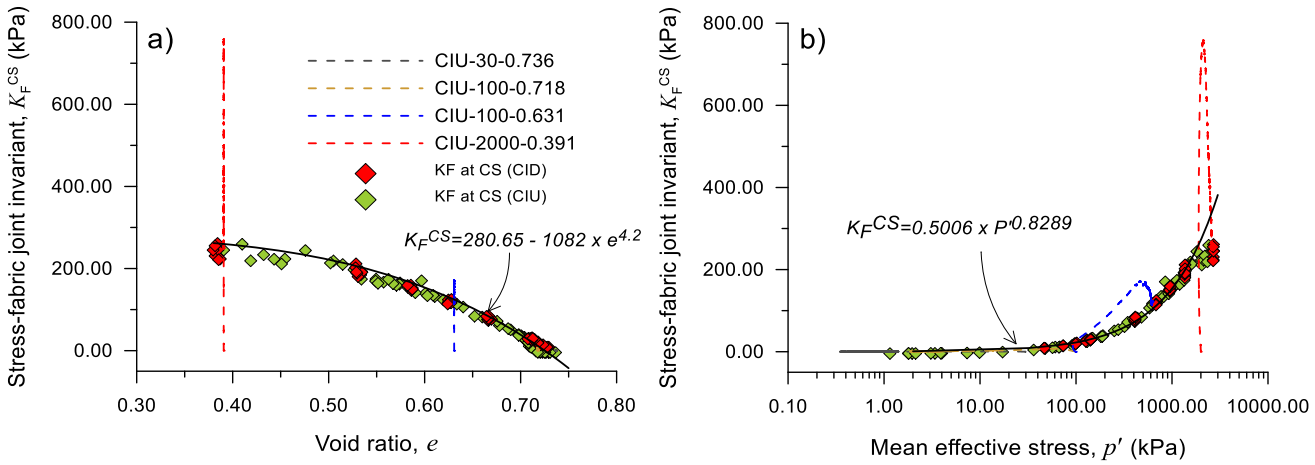

Fig. 7 K_F values at CS and the evolution of K_F during undrained shearing: **a** $K_F - p'$ space; **b** $K_F - e$ space

$$n_{ij} = \frac{s_{ij}}{\sqrt{s_{ij}s_{ij}}} \tag{17}$$

Additionally, von Mises invariant, F_{vm} of fabric tensor proposed by Huang et al. [18] and stress-fabric joint invariant, K_{F}, proposed by Zhao and Guo [91] are also adopted in this study to further investigate the fabric anisotropy and its evolution in DEM. This is further discussed in the following sections (Fig. 7).

3. A pure measure of the relative orientation of the two fabric and stress tenors, A', proposed by Zhao and Guo [91]:

$$A' = n_{ij}^{\mathrm{F}} n_{ij} \tag{18}$$

where, n_{ij} is deviatoric loading direction expressed in Eq. (17) and n_{ij}^{F} is deviatoric fabric direction defined below:

$$n_{ij}^{\mathrm{F}} = \frac{F_{ij}}{\sqrt{F_{ij}F_{ji}}} \tag{19}$$

The correlation between K_F and p' and K_F and e at CS by power-law fitting is shown in Fig. 8a and b. The evolution of K_F during the undrained shearing process for four samples with different confining pressures is also provided to show the stress dependency of the evolution path. A non-linear relationship for both K_F at CS is observed which implies on the uniqueness of CSL and is consistent with the concept of CS as explained in ACST by Li and Dafalias [32].

The fabric evolution during shearing in both drained and undrained tests is studied using the FAV A as defined in Eq. (5). Figure 8a, b indicate that A not only evolved to a CS value (i.e. A = 1) but also first rose beyond CS (slight rise for loose specimen) and only returned to CS at relatively large strains, which is different from the evolution of

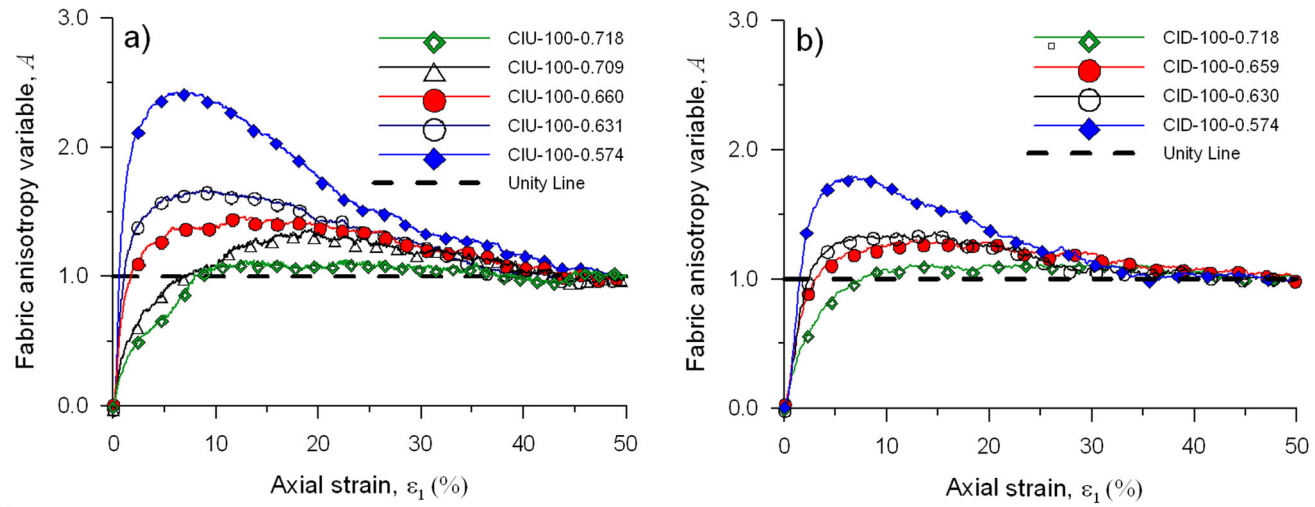

Fig. 8 Evolutions of fabric anisotropy variable for specimens with different densities **a** in undrained tests; **b** in drained tests

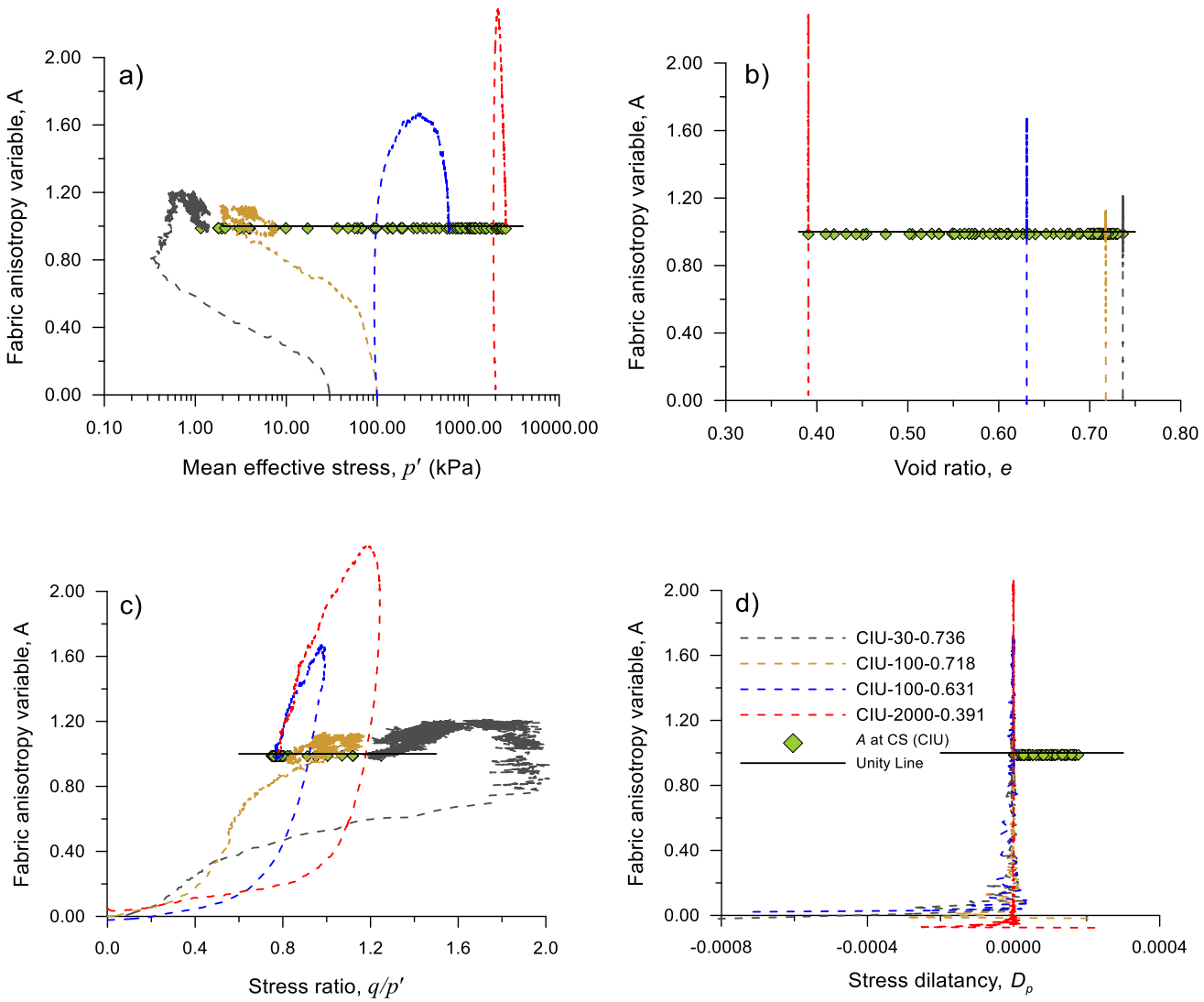

Fig. 9 A values at CS and the evolution of A during undrained shearing: **a** A–p' space; **b** A–e space; **c** A–stress ratio, **d** A–stress dilatancy

A and F originally presented by Li and Dafalias [32]. A similar observation was previously reported for dense samples by Fu and Dafalias [13] and Nguyen et al. [44], and was later quantified by Yang et al. [86].

Figures 9a, b shows the relationships between A and p' and A and e at CS and its evolution path for four samples with different p' during the undrained shearing process. As expected and defined by Li and Dafalias [32], when A approaches the critical state value 1 for both cases. This special behaviour of the critical fabric structure can be further demonstrated through plotting A versus stress ratio $(\eta = q/p')$ and stress dilatancy $(D_P = -\mathrm{d}\varepsilon_v^p/\mathrm{d}\varepsilon_q^p)$, as shown in Figs. 9c, d. Similar evolution of fabric anisotropy was previously reported by Wang et al. [78] and Yuan et al. [89].

A normalised anisotropy variable (A') as defined in Eq. 18 has also been proposed by Zhao and Guo [91] as a pure measurement of the relative orientation of the two fabric and stress tensors. This variable is used in this study to further examine the fabric evolution during the shearing process. The evolution of (A') for five samples with different confining pressures during the undrained shearing process is shown in Fig. 10a, b. The evolution path indicates that the stress and the fabric tensor always tend to become coaxial, and (A') approaches unity shortly after the application of shear and then stays at this value until reaching the CS. This behaviour is also reported by Zhao and Guo [91], which is indeed a very special property of the critical fabric structure and is consistent with Li and Dafalias [32].

However, valuable as it may be, the proposed variable is indeed a normalised quantity of the FAV A and may not be an appropriate parameter to characterise the fabric anisotropies due to the exclusion of fabric intensity

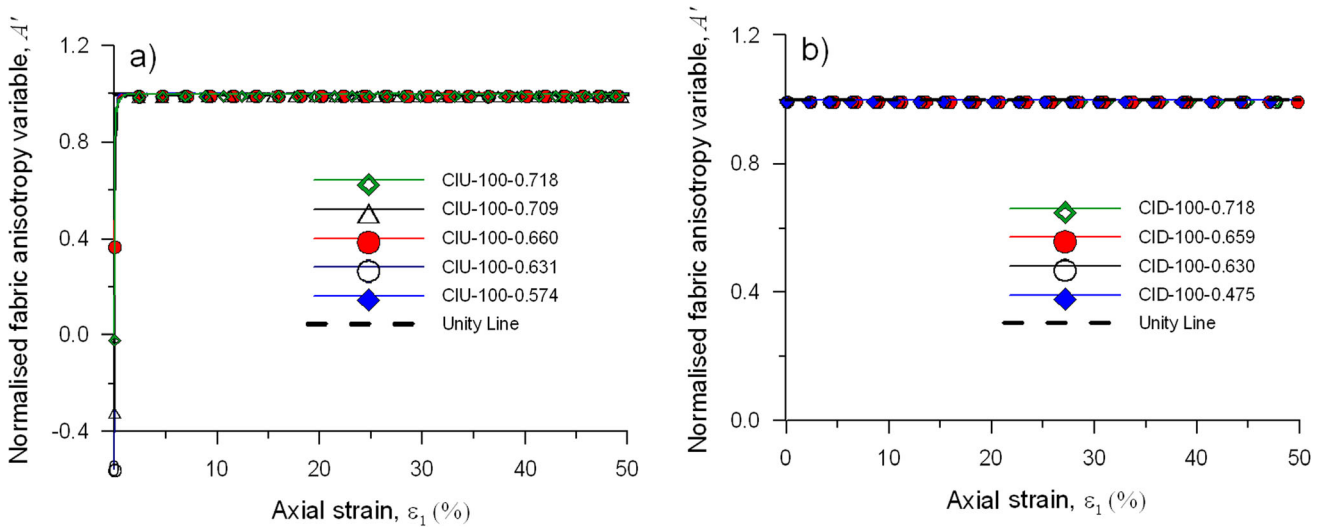

Fig. 10 Evolution of A' during shearing process towards CS at various p'

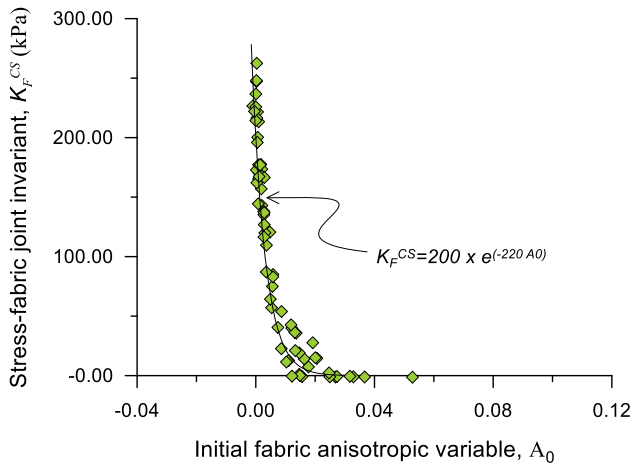

Fig.11 Correlation between initial fabric anisotropy variable and stress fabric joint invariant at CS

($F = \sqrt{F_{ij}F_{ji}}$) from the measurement. It is evident that A tends toward 1 at critical state because both F and A' tend toward 1. Thus, A of Eq. 5 is the fabric variable that in conjunction with stress ratio, η, and void ratio, e, can be used to define the necessary and sufficient conditions for a critical state to occur (i.e. the conditions listed in Eq. (6)).

The correlation between K_F at CS and initial FAV A_0, is shown in Fig. 11. As expected, due to the same nature of both parameters (both defined on the basis of fabric and loading orientation), a unique non-linear relationship is observed. This implies the suitability of FAV A to investigate the degree of anisotropy provided that this micromechanical fabric-based parameter can be incorporated into the constitutive model using DSP ζ and properly linked to the characteristic features of granular soil behaviour.

In addition, it is understood that the FAV A of ACST was purposefully defined to be related to the unit norms with the normal n on the yield surface or even more general (for theories that do not use yield surface, i.e. hypoplasticity), along the plastic strain rate direction n. This would enable the change of A to -A upon reversal of loading (i.e. cyclic loading). Such reversal behaviour is of cardinal importance for the description of the response of sands, i.e. between triaxial compression (dilatant) and extension (static liquefaction). All other relevant indices used in this study (i.e. F_{vM} and K_F) are of restricted value in a theory that must address also the reversal of loading, while they do not change sign upon reversal of stress rate because the stress is still along the direction of the fabric. In addition, it is not possible that these quantities to be correlated to important Dilatancy State parameter DSP ζ. Therefore, the constitutive modelling presented in the following section is based on the FAV A to further explore the effect of fabric within the context of ACST.

3.4 Constitutive formulation

Rahman, Dafalias [57] proposed a new expression of DSP ζ by combing Eqs. (7) and (8), which is presented in the following equation. ζ enables the ACST constitutive model [32] to better account for fabric for prediction of macrobehaviour for Toyoura sand and Sydney sand with silts. However, such a new ζ has not been evaluated yet in the light of micromechanics and fabric entities.

$$\zeta = \psi - e_A \frac{\langle e_{\lim} - e \rangle}{(e_{\lim} - e_{CS})}(A-1) \tag{20}$$

An attempt is made in this study for the first time to calculate the initial dilatancy state parameter, DSP (ζ_{0-DEM}), from micromechanical entities of this DEM Study. For this, the initial FAV A_0 was calculated using the initial values of the unit-norm deviatoric tensor n_{ij} (Eq. (17)) and deviatoric fabric tensor F_{ij} (Eq. (13)). To evaluate the performance of Eq. (20), it was compared with ζ_{0-CM} was calculated by constitutive formulation (CM) as outlined below.

F_{ij} is a second-order fabric tensor representing the anisotropic geometry of the internal structure in soil. For an initially cross-anisotropic sample with the isotropic plane coinciding with the $x_2 - x_3$ plane and the axis of anisotropy aligning with the x_1-axis, Zhao and Guo [91] proposed the following expression for F_{ij}:

$$F_{ij} = \begin{bmatrix} F_{11} & 0 & 0 \\ 0 & F_{22} & 0 \\ 0 & 0 & F_{33} \end{bmatrix} = \sqrt{\frac{2}{3}} \begin{bmatrix} F_0 & 0 & 0 \\ 0 & -F_0/2 & 0 \\ 0 & 0 & -F_0/2 \end{bmatrix} \tag{21}$$

where, F_0 can be obtained according to equation below

$$F_0 = \frac{3\sqrt{6}(2\upsilon - 1)}{3(1-2\upsilon) + (dq/dp)(\upsilon - 2)} \tag{22}$$

ν is the Poisson's ratio ($0 < \nu < 0.5$) for DEM specimen.

As part of this study, a sensitivity analysis considering the material orthotropy has been carried out to select suitable values for Poisson's ratio and as a result of which, the constitutive model outputs using Poisson's ratios ranging from 0.46 to 0.48 show a reasonably good consistency with DEM results. The possible explanation for such a great range of values in Poisson's ratio probably lies in a very high particle stiffness in the DEM specimen.

The deviatoric unit loading direction tensor n_{ij} can be expressed as:

$$n_{ij} = \frac{N_{ij} - N_{mn}\delta_{mn}\delta_{ij}/3}{\|N_{ij} - N_{mn}\delta_{mn}\delta_{ij}/3\|}, N_{ij} = \frac{\partial \widetilde{f}}{\partial r_{ij}}, \widetilde{f} = R/g(\theta) \tag{23}$$

$g(\theta)$ is an interpolation function based on the Lode angle θ of r_{ij} as follows:

$$g(\theta) = \frac{\sqrt{(1+c^2)^2 + 4c(1-c^2)\sin 3\theta} - (1+c^2)}{2(1-c)\sin 3\theta} \tag{24}$$

where $c = M_e/M_c$ which is the ratio between the critical state stress ratio in triaxial extension (M_e); and that in triaxial compression (M_e); and

$$\theta = -\frac{\left[\sin^{-1}\left(9R'/2R^3\right)\right]}{3} \text{ with } R' = r_{ij}r_{jk}r_{ki} = tr(r^3) - tr(r^2)tr(r) + \frac{2}{9(tr(r))^3} \tag{25}$$

$$R = \sqrt{3/2 r_{ij} r_{ij}} \text{with} r_{ij} = \frac{\sigma'_{ij} - p'\delta_{ij}}{p'} = s_{ij}/p' \tag{26}$$

Following the determination of F_{ij} and n_{ij}, initial FAV A_0 was calculated using Eq. (5) and initial DSP (ζ_0) were calculated using Eq. (20).

The scatter graph of initial FAV A_0 and initial ζ_0 based on CM and based on DEM are presented in Fig. 12. As can be seen in Fig. 12a, the initial FAV A_0 ranges from − 0.1 to 0.1 for both CM and DEM. Based on Fig. 12b, there is a good agreement between CM- and DEM-derived values and the best-fit relation is actually the line of equality which indicates that the Eq. (20) by Rahman, Dafalias [57] is likely to provide a reliable method to estimate DSP ζ.

It should be mentioned that Eq. (20) is based on a simple form of rate equation for the fabric tensor ($dF = \langle\lambda\rangle c(N - F) = c(\pm 1 - F)|d\varepsilon_q^p|$) in the sense that it does not allow for the fabric norm to increase above 1 as observed in DEM studies for dense samples (Fu and Dafalias [13]), and which requires the introduction of an additional parameter $r < 1$ in front of F that becomes 1 at CS (Li and Dafalias [32]). Note, while the use of the above rate equation in terms of λ and $d\varepsilon_q^p$ is common in the literature (Gao et al. [15]; Zhao and Kruyt [92]), there are other approaches found in the literature, e.g. combining λ and dilatancy (Wang et al. [78]; Yang et al. [86]), stress ratio rate and e (Lashkari and Latifi [27]; Wan and Guo [77]), strain rate and e (Fang et al. [12], Sun and Sundaresan [71]). While further investigation is necessary in regard to the evolution equation for the fabric tensor, in this paper Eq. (20) has been adopted in order to focus on the main objective of the constitutive relation between microstructures and macroscopic behaviour of granular soils (Fig. 13).

3.5 State parameters and fabric evolution

Previously published works [44, 59, 85] indicate that the behaviour of granular materials can be characterised by the initial classic state parameter (ψ_0). Therefore, it can be of particular interest in this study to examine if the same property can be seen for initial DSP ζ_0. Correlation between instability stress ratio η_{IS}, and initial ψ_0 and ζ_0 are plotted in Fig. 13 with their best-fit relation presented by $\eta_{IS} = 0.4805 \times \exp(-10.54\psi_0)$ and $\eta_{IS} = 0.7085 \times \exp(-21.77\zeta_0)$, respectively. Based on a comparison between coefficients of determination, denoted R^2, the relation between η_{IS} and initial state parameter has

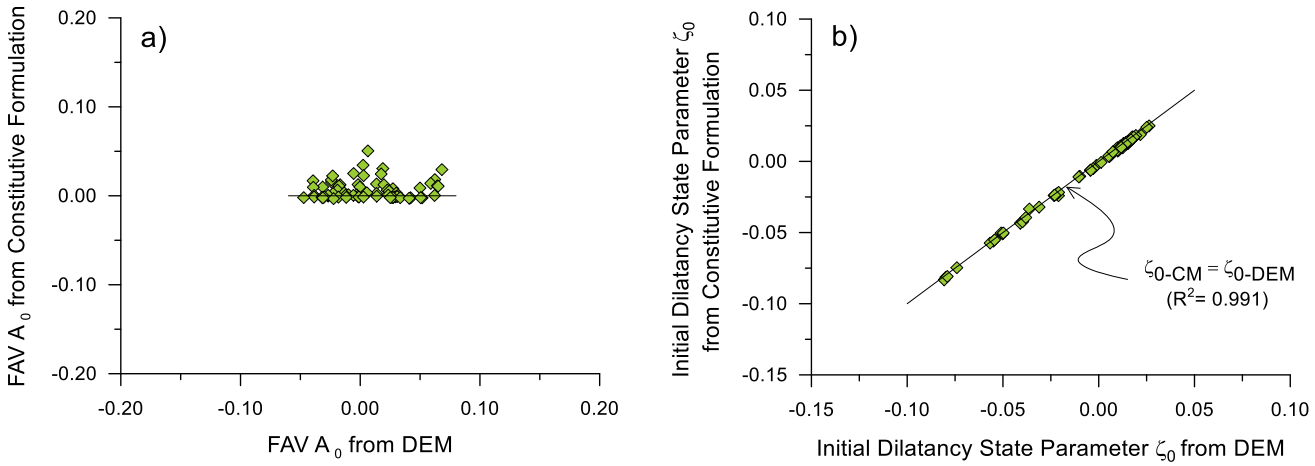

Fig. 12 Scatter graph of **a** initial FAV A_0 and **b** initial DSP ζ_0 based on CM and based on DEM

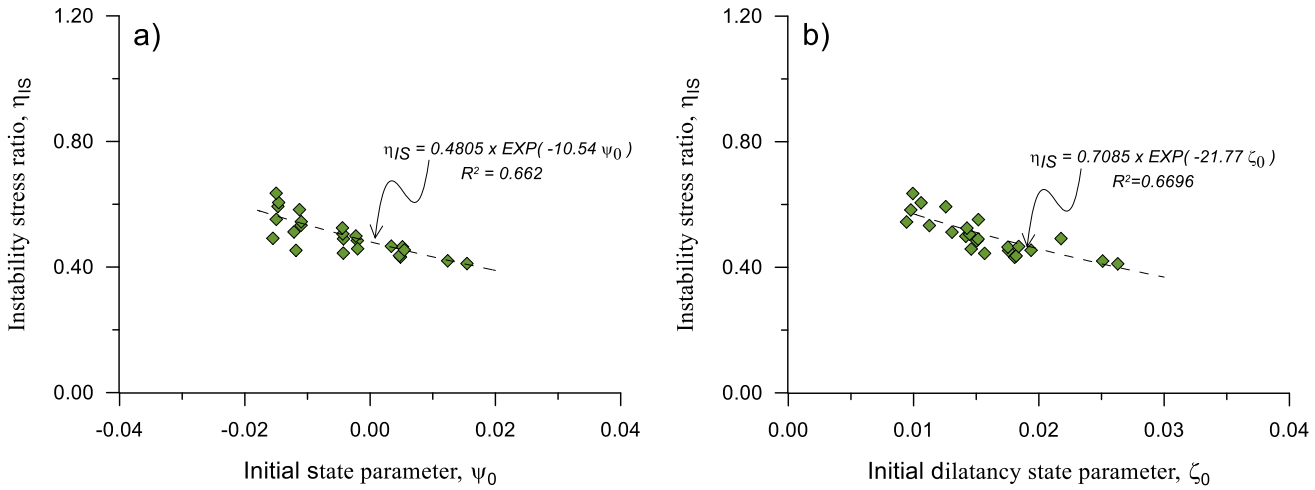

Fig. 13 Correlation between instability stress ratio and **a** initial state parameter; **b** initial dilatancy state parameter

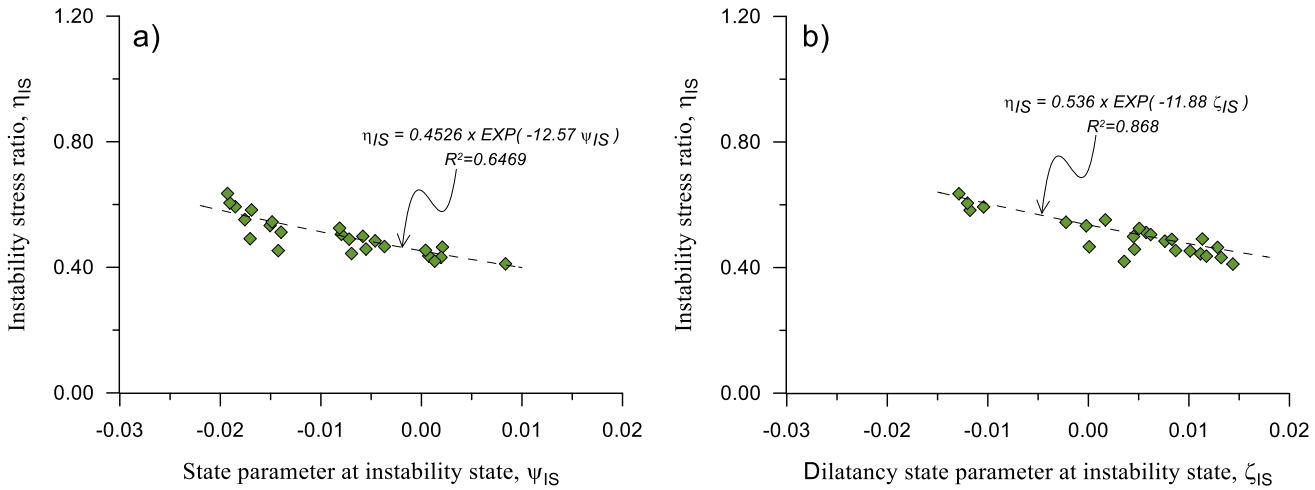

Fig. 14 Correlation between instability stress ratio at **a** state parameter at instability state; **b** dilatancy state parameter at instability state

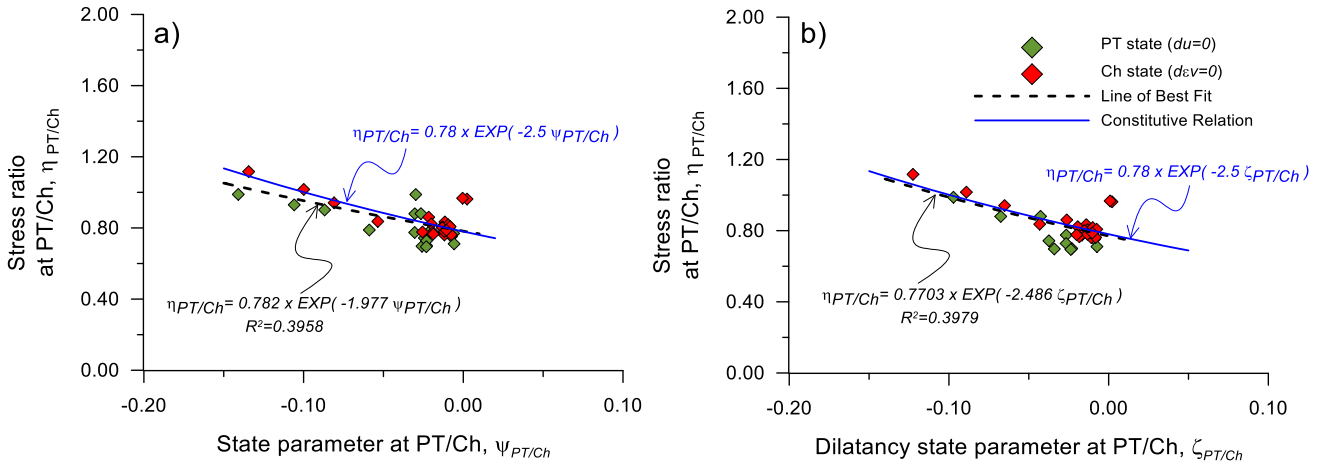

Fig. 15 Correlation between stress ratio at PT/Ch with **a** state parameter at PT/Ch; **b** dilatancy state parameter at PT/Ch

slightly been improved using ζ_0. This can be attributed to the inclusion of fabric entities in our model. It is expected that similar or better correlations can be identified between the stress ratio and state parameter at the same state.

The correlation between stress ratio and state parameters at instability state were also examined in this study which would be of more use to future fabric-based constitutive modelling. Figure 14 indicates that there is a reasonable trend between stress ratio and classic or dilatancy state parameters at the instability state, which is presented by the best-fit relations of $\eta_{IS} = 0.4526 \times \exp(-12.57\psi_{\mathrm{IS}})$ and $\eta_{IS} = 0.536 \times \exp(-11.88\zeta_{\mathrm{IS}})$. Based on a comparison between R^2 coefficients, the identified correlation between stress ratio and state parameter at instability has considerably been improved using ζ_{IS} which may be related to the inclusion of fabric in dilatancy state parameter.

The correlation between state parameters and stress ratio at phase transformation (PT) in undrained and at characteristic state (Ch) in drained tests are shown in Fig. 15. The best-fit relation can be presented by $\eta_{\mathrm{PT/Ch}} = 0.782 \times \exp(-1.977\psi_{\mathrm{PT/Ch}})$ and $\eta_{\mathrm{PT/Ch}} = 0.7703 \times \exp(-2.486\zeta_{\mathrm{PT/Ch}})$ in which the state dependent dilatancy was elaborated. As can be seen, this relation has been presented using a single trend suggesting that the PT and Ch are likely representing the same characteristic of granular soil behaviour but in different drainage conditions, which is consistent with previous observations by Nguyen et al. [45]. A similar exponential relation was proposed by Li and Dafalias [31, 32], respectively, for both classic and dilatancy state parameters expressed by $\eta_{\mathrm{PT/Ch}} = M \times \exp(m\psi_{\mathrm{PT/Ch}})$ and $\eta_{\mathrm{PT/Ch}} = M \times \exp(m\zeta_{\mathrm{PT/Ch}})$. These constitutive relations are also plotted in Fig. 15 in which $m = -2.5$. As expected, based on the consistency between the best-fit curves and constitutive relations as well as a comparison between R^2 coefficients, a better correlation can be seen between $\eta_{\mathrm{PT/Ch}}$ and $\zeta_{\mathrm{PT/Ch}}$. Although there is only a marginal improvement in the comparison of the best-fit curves, when viewed from the perspective of constitutive modelling and considering the correlation between $\eta_{\mathrm{PT/Ch}} = M \times \exp(m\zeta_{\mathrm{PT/Ch}})$ and the best-fit curves, a noticeable improvement can be seen which can be attributed to the inclusion of fabric in dilatancy state parameter.

3.6 Conclusions

The micromechanical and macromechanical characteristic features of the behaviour under drained and undrained conditions were examined using DEM simulations. The major findings are:

- The state-dependent behaviours of granular soil were observed for loose, medium dense and dense specimens. This includes contraction and static liquefaction in very loose soil, quasi-steady state or phase transformation (PT) in medium-dense soil, and dilatancy and hardening in dense soil. All the specimens reach a unique CSL in the p'-q-e space regardless of the initial density, confining pressure and loading mode.
- The initial mechanical coordination number Z_{m} increases with decreasing initial void ratio e_0. However, there is no unique correlation between Z_{m} and e, although to some degree Z_{m} reflects the soil density. It is found that the critical Z_{m} value linearly depends on the critical p' value. Meanwhile, the critical Z_{m} value is generally smaller than the initial one, although the density or p' value at the critical state may increase when compared with the initial one. Moreover, the quasi-steady state corresponds to the minimum Z_{m} value during shearing, and the static liquefaction happens when the Z_{m} value is less than 8.

- It was also found that the micromechanical measures, F_{vM} and K_F, evolved toward CS at high ε_1. The CS values of these micromechanical quantities from drained and undrained simulations all terminated in a single line (CSL).
- A unique relationship between stress ratio at PT/Ch state ($\eta_{PT/Ch}$) and classic and dilatancy state parameters ($\psi_{PT/Ch}$ and $\zeta_{PT/Ch}$) was established. The uniqueness of this relationship implies that the PT and Ch are likely representing the same transition state of granular soil behaviour but in different drainage conditions. However, this unique relationship cannot properly be detected in microscale by plotting the von Mises fabric, F_{vm} against ψ and ζ at PT/Ch state, which can be associated to the definition of undrained and drained conditions in DEM simulation.
- The correlation between stress ratio and both classic and dilatancy state parameter (ψ and ζ) were studied in important characteristic features (e.g. instability, phase transformation and characteristic state). This correlation was improved using DSP ζ which might be due to the inclusion of fabric in our model. This observation is new and significant for modelling fabric evolution. This represents a novel contribution to the understanding of anisotropic responses in constitutive modelling. Additionally, this study deviates from the linear variation of η_{PT} with ψ found in previous works, such as Manzari and Dafalias [38]. The exponential correlations presented, while closely resembling linearity, exhibit better behaviour, adding a layer of sophistication to the existing knowledge in this domain.

The findings and recommendations contained within this study are the results of observations from DEM simulations and a comprehensive review of pertinent literature. To the best of authors' knowledge, they provide a plausible interpretation of both micromechanical and macromechanical behaviours exhibited by granular materials. This enhanced understanding contributes significantly to the quantitative knowledge essential for advancing future constitutive modelling efforts. To validate and enhance the robustness of these findings, additional observations using experimental approaches can be pursued.

Appendix

The effect of number of particles, NP

Rigid boundaries may inflict uncharacteristically large friction angles in small assemblies and therefore the accuracy and consistency of results may depend on the specimen size (Zhao and Guo [91]; Huang et al. [18]. The specimen size (or number of particles, N_P) should be large enough to minimise the influence of the end-restraint conditions. The q–ε_1 and q–p' responses for undrained simulations with different number of particles of 13,570 and 25,750 are presented in Fig. 16a and b. Despite the

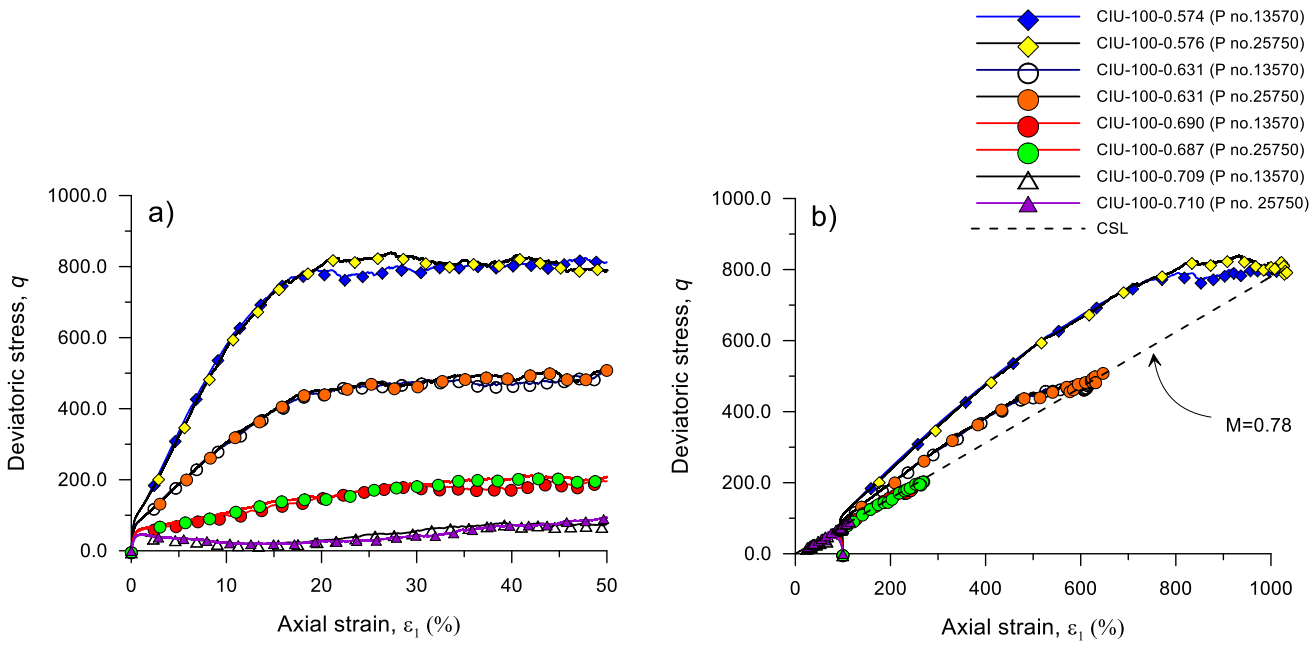

Fig. 16 Effect of number of particles, N_P, on undrained behaviour: **a** q–ε_1 space; **b** q–p' space

large difference of N_P, two pairs of simulations with exactly the same p' and almost the same e_0 exhibited similar responses. The slight difference in their responses is due to slight variations of their e_0 since it is difficult to achieve exactly the same e_0. Similar observations have been reported by Ng [43] and Nguyen et al. [44] for specimens with a range of ellipsoid particles varying from 863 to 1170 and 1450 to 5400, respectively. The smaller number of particles has been adopted in this study to avoid unnecessary computation in the simulation.

Acknowledgements The first author would like to acknowledge the Australian Government Research Training Program scholarship scheme for funding this research.

Funding Open Access funding enabled and organized by CAUL and its Member Institutions.

Data availability Data generated or analysed during the study are available from the corresponding author by request.

Declarations

Conflict of interest The authors declare that they have no conflict of interest.

Ethical approval This article does not contain any studies with human participants or animals performed by any of the authors.

References

1. Alonso-Marroquin F, Luding S, Herrmann H, Vardoulakis I (2005) Role of anisotropy in the elastoplastic response of a polygonal packing. Phys Rev E 71(5):051304
2. Baki MAL, Rahman MM, Lo SR (2014) Predicting onset of cyclic instability of loose sand with fines using instability curves. Soil Dyn Earthq Eng 61–62:140–151. https://doi.org/10.1016/j.soildyn.2014.02.007
3. Baki MAL, Rahman MM, Lo SR, Gnanendran CT (2012) Linkage between static and cyclic liquefaction of loose sand with a range of fines contents. Can Geotech J 49(8):891–906. https://doi.org/10.1139/t2012-045
4. Been K, Jefferies MG (1985) A state parameter for sands. Géotechnique 35(2):99–112
5. Bobei DC, Lo SR, Wanatowski D, Gnanendran CT, Rahman MM (2009) Modified state parameter for characterizing static liquefaction of sand with fines. Can Geotech J 46(3):281–295. https://doi.org/10.1139/t08-122
6. Cambou B, Dubujet P, Nouguier-Lehon C (2004) Anisotropy in granular materials at different scales. Mech Mater 36(12):1185–1194
7. Castro G (1975) Liquefaction and cyclic mobility of saturated sands. J Geotech Eng Div 101(6):551–569
8. Christoffersen J, Mehrabadi M, Nemat-Nasser S (1981) A micromechanical description of granular material behavior. J Appl Mech 48(2):339–344
9. Dafalias YF, Manzari M (2004) Simple plasticity sand model accounting for fabric change effects. J Eng Mech 130(6):622–634. https://doi.org/10.1061/(ASCE)0733-9399(2004)130:6(622)
10. Dafalias YF, Papadimitriou A, Li X (2004) Sand plasticity model accounting for inherent fabric anisotropy. J Eng Mech 130(11):1319–1333. https://doi.org/10.1061/(ASCE)0733-9399(2004)130:11(1319)
11. Duran J (2012) Sands, powders, and grains: an introduction to the physics of granular materials. Springer Science & Business Media, Berlin
12. Fang H, Shen Y, Zhao Y (2019) Multishear bounding surface modelling of anisotropic sands accounting for fabric and its evolution. Comput Geotech 110:57–70. https://doi.org/10.1016/j.compgeo.2019.02.015
13. Fu P, Dafalias YF (2011) Fabric evolution within shear bands of granular materials and its relation to critical state theory. Int J Numer Anal Meth Geomech 35(18):1918–1948. https://doi.org/10.1002/nag.988
14. Gajo A, Wood M (1999) Trent sand: a kinematic-hardening constitutive model: the q-p formulation. Geotechnique 49(5):595–614. https://doi.org/10.1680/geot.1999.49.5.595
15. Gao Z, Zhao J, Li X-S, Dafalias YF (2014) A critical state sand plasticity model accounting for fabric evolution. Int J Numer Anal Meth Geomech 38(4):370–390. https://doi.org/10.1002/nag.2211
16. Gu X, Huang M, Qian J (2013) Dem investigation on the evolution of microstructure in granular soils under shearing. Granular Matter 16(1):91–106. https://doi.org/10.1007/s10035-013-0467-z
17. Guo N, Zhao J (2013) The signature of shear-induced anisotropy in granular media. Comput Geotech 47:1–15. https://doi.org/10.1016/j.compgeo.2012.07.002
18. Huang X, Hanley KJ, O'Sullivan C, Kwok CY (2014) Exploring the influence of interparticle friction on critical state behaviour using dem. Int J Numer Anal Meth Geomech 38(12):1276–1297
19. Ishihara K (1993) Liquefaction and flow failure during earthquakes. Geotechnique 43(3):351–415
20. Ishihara H, Kase S (1975) Studies on melt spinning. V. Draw resonance as a limit cycle. J Appl Polym Sci 19(2):557–566
21. Itasca CGI (2009) Itasca: Particle flow code (pfc3d) manual. Itasca Consulting Group Inc., Minn
22. Jefferies MG (1993) Nor-sand: a simple critical state model for sand. Geotechnique 43(1):91–103
23. Jiang M, Konrad J, Leroueil S (2003) An efficient technique for generating homogeneous specimens for dem studies. Comput Geotech 30(7):579–597
24. Kanatani K-I (1984) Stereological determination of structural anisotropy. Int J Eng Sci 22(5):531–546
25. Karimi M, Lashkari A, Binesh SM (2015) Evaluating the effect of fines on critical state behaviour of binary packing soils using dem. Paper presented at the The first national conference on sustainable development in construction with environmental approach, Shiraz,
26. Klotz E, Coop M (2001) An investigation of the effect of soil state on the capacity of driven piles in sands. Géotechnique 51(9):733–751

27. Lashkari A, Latifi M (2008) A non-coaxial constitutive model for sand deformation under rotation of principal stress axes. Int J Numer Anal Meth Geomech 32(9):1051–1086. https://doi.org/10.1002/nag.659
28. Lashkari A, Shourijeh PT, Khorasani SSS, Irani N, Rahman MM (2022) Effects of overconsolidation history on flow instability of clean and silty sands. Acta Geotechnica 17(11):4989–5007
29. Lätzel M, Luding S, Herrmann HJ (2000) Macroscopic material properties from quasi-static, microscopic simulations of a two-dimensional shear-cell. Granular Matter 2(3):123–135
30. Li X (2006) Micro-scale investigation of the quasi-static behavior of granular material. The Hong Kong University of Science and Technology, Hong Kong
31. Li XS, Dafalias YF (2000) Dilatancy for cohesionless soils. Geotechnique 50(4):449–460
32. Li XS, Dafalias YF (2012) Anisotropic critical state theory: role of fabric. J Eng Mech 138(3):263–275. https://doi.org/10.1061/(asce)em.1943-7889.0000324
33. Li X, Li XS (2009) Micro-macro quantification of the internal structure of granular materials. J Eng Mech 135(7):641–56
34. Li XS, Wang Y (1998) Linear representation of steady-state line for sand. J Geotech Geoenviron Eng 124(12):1215–1217
35. Li X, Yu HS, Li XS (2009) Macro–micro relations in granular mechanics. Int J Solids Struct 46(25–26):4331–41
36. Lu Y, Frost D (2010) Three-dimensional dem modeling of triaxial compression of sands. Paper presented at the GeoShanghai 2010 international conference, Shanghai, China,
37. Luding S (2010) Macroscopic stress from dynamic, rotating granular media. In: AIP Conference Proceedings, Vol. 1227, No. 1, pp. 208–213. American Institute of Physics
38. Manzari MT, Dafalias YF (1997) A critical state two-surface plasticity model for sands. Geotechnique 47(2):255–272
39. Masson S, Martinez J (2001) Micromechanical analysis of the shear behavior of a granular material. J Eng Mech 127(10):1007–1016
40. Minh N, Cheng Y (2013) A dem investigation of the effect of particle-size distribution on one-dimensional compression. Géotechnique 63(1):44
41. Mitchell JK, Soga K (2005) Fundamentals of soil behavior. Wiley, New york
42. Nakata Y, Hyodo M, Murata H, Yasufuku N (1998) Flow deformation of sands subjected to principal stress rotation. Soils Found 38(2):115–128
43. Ng T-T (2004) Triaxial test simulations with discrete element method and hydrostatic boundaries. J Eng Mech 130(10):1188–1194
44. Nguyen H, Rahman M, Fourie A (2017) Undrained behaviour of granular material and the role of fabric in isotropic and k 0 consolidations: Dem approach. Géotechnique 67:1–15
45. Nguyen H, Rahman M, Fourie A (2018) Characteristic behavior of drained and undrained triaxial compression tests: Dem study. J Geotech Geoenviron Eng 144(9):04018060
46. Nguyen HBK, Rahman MM, Fourie AB (2021) How particle shape affects the critical state, triggering of instability and dilatancy of granular materials—results from a dem study. Geotechnique 71(9):749–764. https://doi.org/10.1680/jgeot.18.P.211
47. Oda M (1972) The mechanism of fabric changes during compressional deformation of sand. Soils Found 12(2):1–18
48. Oda M (1972) Initial fabrics and their relations to mechanical properties of granular material. Soils Found 12(1):17–36
49. Oda M (1982) Fabric tensor for discontinuous geological materials. Soil found 22(4):96–108
50. Oda M, Iwashita K (1999) An introduction mechanics of granular materials. AA BALKEMA, Amsterdam
51. Oda M, Iwashita K (2000) Study on couple stress and shear band development in granular media based on numerical simulation analyses. Int J Eng Sci 38(15):1713–1740
52. Oda M, Nemat-Nasser S, Konishi J (1985) Stress-induced anisotropy in granular masses. Soils Found 25(3):85–97
53. Potyondy D, Cundall P (2004) A bonded-particle model for rock. Int J Rock Mech Min Sci 41(8):1329–1364
54. Poulos HG (1971) Behavior of laterally loaded piles i. Single piles. J Soil Mech Found Div 97(5):711–731
55. Poulos SJ (1981) The steady state of deformation. J Geotech Geoenviron Eng 107(5):553–562
56. Rahman MM, Baki M, Lo S (2014) Prediction of undrained monotonic and cyclic liquefaction behavior of sand with fines based on the equivalent granular state parameter. Int J Geomech 14(2):254–266. https://doi.org/10.1061/(ASCE)GM.1943-5622.0000316
57. Rahman MM, Dafalias YF (2022) Modelling undrained behaviour of sand with fines and fabric anisotropy. Acta Geotech 17(6):2305–2324. https://doi.org/10.1007/s11440-021-01410-7
58. Rahman MM, Lo SR (2012) Predicting the onset of static liquefaction of loose sand with fines. J Geotech Geoenviron Eng 138(8):1037–1041. https://doi.org/10.1061/(ASCE)GT.1943-5606.0000661
59. Rahman MM, Lo S (2014) Undrained behavior of sand-fines mixtures and their state parameter. J Geotech Geoenviron Eng 140(7):04014036
60. Rahman MM, Lo SR, Baki MAL (2011) Equivalent granular state parameter and undrained behaviour of sand-fines mixtures. Acta Geotechnica 6(4):183–194
61. Rahman MM, Nguyen HBK, Fourie AB, Kuhn MR (2021) Critical state soil mechanics for cyclic liquefaction and postliquefaction behavior: Dem study. J Geotech Geoenviron Eng 147(2):04020166. https://doi.org/10.1061/(ASCE)GT.1943-5606.0002453
62. Rahman MM, Nguyen HBK, Rabbi ATMZ (2018) The effect of consolidation on undrained behaviour of granular materials: experiment and dem simulation. Geotech Res 5(4):199–217. https://doi.org/10.1680/jgere.17.00019
63. Rahman MM, Sitharam TG (2020) Cyclic liquefaction screening of sand with non-plastic fines: critical state approach. Geosci Front 11(2):429–438
64. Roscoe KH, Schofield A, Wroth C (1958) On the yielding of soils. Geotechnique 8(1):22–53
65. Rothenburg L, Bathurst R (1989) Analytical study of induced anisotropy in idealized granular materials. Geotechnique 39(4):601–614
66. Rothenburg L, Kruyt NP (2004) Critical state and evolution of coordination number in simulated granular materials. Int J Solids Struct 41:5763–5774
67. Satake M (1978) Constitution of mechanics of granular materials through the graph theory. Continuum Mech Stat Appr Mech Granul Mater 41:47–62
68. Schofield A, Wroth P (1968) Critical state soil mechanics. McGraw-hill, London
69. Sitharam T, Dinesh S, Shimizu N (2002) Micromechanical modelling of monotonic drained and undrained shear behaviour of granular media using three-dimensional dem. Int J Numer Anal Meth Geomech 26(12):1167–1189
70. Soga K (2010) Microscopic characterisation of soils. University of Cambridge, Cambridge
71. Sun JIN, Sundaresan S (2011) A constitutive model with microstructure evolution for flow of rate-independent granular materials. J Fluid Mech 682:590–616. https://doi.org/10.1017/jfm.2011.251

72. Sykut J, Molenda M, Horabik J (2008) Dem simulation of the packing structure and wall load in a 2-dimensional silo. Granular Matter 10(4):273–278
73. Thornton C, Zhang L (2010) On the evolution of stress and microstructure during general 3d deviatoric straining of granular media. Geotechnique 60(5):333–341
74. Tordesillas A, Muthuswamy M (2009) On the modeling of confined buckling of force chains. J Mech Phys Solids 57(4):706–727
75. Vairaktaris E, Theocharis AI, Dafalias YF (2020) Correlation of fabric tensors for granular materials using 2d dem. Acta Geotech 15:681–694
76. Verdugo R, Ishihara K (1996) The steady state of sandy soils. Soils Found 36(2):81–91
77. Wan RG, Guo PJ (2004) Stress dilatancy and fabric dependencies on sand behavior. J Eng Mech 130(6):635–645. https://doi.org/10.1061/(ASCE)0733-9399(2004)130:6(635)
78. Wang R, Dafalias YF, Fu P, Zhang J-M (2020) Fabric evolution and dilatancy within anisotropic critical state theory guided and validated by dem. Int J Solids Struct 188–189:210–222. https://doi.org/10.1016/j.ijsolstr.2019.10.013
79. Wang Z-L, Dafalias YF, Li X-S, Makdisi FI (2002) State pressure index for modeling sand behavior. J Geotech Geoenviron Eng 128(6):511–519
80. Wang R, Fu P, Zhang J-M, Dafalias YF (2016) Dem study of fabric features governing undrained post-liquefaction shear deformation of sand. Acta Geotech 11:1321–1337
81. Wood DM, Belkheir K, Liu DF (1994) Strain softening and state parameter for sand modelling. Geotechnique 44(2):335–339
82. Wood DM, Maeda K (2008) Changing grading of soil: effect on critical states. Acta Geotech 3(1):3–14
83. Wu Q, Zheng J, Yang Z (2023) Effects of initial fabric anisotropy on the undrained rotational shear responses of granular material using discrete element simulations. Acta Geotechnica 18:1–20
84. Yan WM, Dong J (2011) Effect of particle grading on the response of an idealized granular assemblage. Int J Geomech 11(4):276–285. https://doi.org/10.1061/(asce)gm.1943-5622.0000085
85. Yang J (2002) Non-uniqueness of flow liquefaction line for loose sand. Géotechnique 52(10):757–760
86. Yang ZX, Xu TT, Chen YN (2018) Unified modeling of the influence of consolidation conditions on monotonic soil response considering fabric evolution. J Eng Mech 144(8):04018073. https://doi.org/10.1061/(ASCE)EM.1943-7889.0001499
87. Yimsiri S, Soga K (2010) Dem analysis of soil fabric effects on behaviour of sand. Géotechnique 60(6):483–495. https://doi.org/10.1680/geot.2010.60.6.483
88. Yoshimine M, Ishihara K, Vargas W (1998) Effects of principal stress direction and intermediate principal stress on undrained shear behavior of sand. Soils Found 38(3):179–188
89. Yuan R, Yu H-S, Yang D-S, Hu N (2019) On a fabric evolution law incorporating the effects of b-value. Comput Geotech 105:142–154. https://doi.org/10.1016/j.compgeo.2018.09.019
90. Zhang J, Lo SCR, Rahman MM, Yan J (2018) Characterizing monotonic behavior of pond ash within critical state approach. J Geotech Geoenviron Eng 144(1):04017100
91. Zhao J, Guo N (2013) Unique critical state characteristics in granular media considering fabric anisotropy. Géotechnique 63(8):695–704
92. Zhao C-F, Kruyt NP (2020) An evolution law for fabric anisotropy and its application in micromechanical modelling of granular materials. Int J Solids Struct 196–197:53–66. https://doi.org/10.1016/j.ijsolstr.2020.04.007
93. Zhou Z, Wang H, Jiang M (2023) Micromechanical mechanism-based anisotropic strength criteria for regularly arranged elliptical particle assembly. Acta Geotechnica. https://doi.org/10.1007/s11440-023-02109-7